

Oxygen Reduction Catalysts

Dinuclear Cobalt Complexes with a Decadentate Ligand Scaffold: Hydrogen Evolution and Oxygen Reduction Catalysis

Carlo Di Giovanni,^[a] Carolina Gimbert-Suriñach,^[a] Michael Nippe,^[b, c, e] Jordi Benet-Buchholz,^[a] Jeffrey R. Long,^{*,[b, c]} Xavier Sala,^{*,[d]} and Antoni Llobet^{*,[a, d]}

Abstract: A new decadentate dinucleating ligand containing a pyridazine bridging group and pyridylic arms has been synthesized and characterized by analytical and spectroscopic techniques. Four new dinuclear cobalt complexes featuring this ligand have been prepared and thoroughly characterized both in the solid state (X-ray diffraction) and in solution (1D and 2D NMR spectroscopy, ESI-MS, and electro-

chemical techniques). The flexible but stable coordination environment provided by the ligand scaffold when coordinating Co in different oxidation states is shown to play a crucial role in the performance of the set of complexes when tested as catalysts for the photochemical hydrogen evolution reaction (HER) and chemical oxygen reduction reaction (ORR).

Introduction

Multielectron reductions such as the oxygen reduction reaction (ORR) and the hydrogen evolution reaction (HER) play an important role in the development of a sustainable energy economy. The former is the cathodic reaction in proton exchange membrane hydrogen fuel cells, the latter is the reductive half reaction of water splitting, which could produce clean and renewable hydrogen fuel. Transition-metal complexes can store electrons through multiple redox states and are therefore excellent candidates to efficiently catalyze these types of reactions. In particular, tetra- and pentadentate polypyridine ligands have been shown to stabilize mononuclear cobalt complexes with high activity in both photo- and electrocatalytic HER systems (Figure 1, top).^[1] This type of ligand provides

labile sites for substrate coordination and high stability towards decomposition in aqueous conditions.

On the other hand, the use of multimetallic complexes can provide a useful tool to enhance the catalytic activity of transition-metal complexes by placing two or more metal centers in proximity to each other, potentially inducing cooperative effects. To this end, we recently reported a dinuclear complex that is able to catalyze the HER in acetonitrile with cobaltocene as the electron donor and trifluoroacetic acid as the proton source (**1**⁴⁺, Figure 1).^[2] The related peroxo complex **2**³⁺ in Figure 1 was found to be active in the four-electron reduction of oxygen (ORR) to water in the presence of octamethylferrocene (Me₈Fc) as the electron donor.^[3] As an expansion of our strategy, we present here a dinucleating ligand based on a pyridazine bridging group, which provides discrete binding sites for two metal centers as well as facilitates potential electronic communication between them (**L**, Figure 1). The pyridazine group has been shown to coordinate two metal centers in numerous dinuclear transition-metal complexes, including those of cobalt(II), cobalt(III), nickel(II), and copper(II).^[4] The decadentate ligand **L** has been designed to furnish a flexible and stable scaffold for the coordination of cobalt in different oxidation states and, thus, produce active catalysts for the HER and ORR.

Results and Discussion

Synthesis and characterization of ligand **L** and complexes **3–6**

The reaction between 3,6-bis(tosyloxymethyl)pyridazine^[6] and *N*-(2-pyridinylmethyl)amine^[7] in the presence of an excess of Na₂CO₃ afforded ligand **L** in 44% yield (Scheme 1). Ligand **L** presents C_{2v} symmetry as confirmed by the ¹H NMR spectrum (Figure S1 in the Supporting Information) and provides five coordination sites per metal center, leaving a sixth site free to ac-

[a] Dr. C. Di Giovanni, Dr. C. Gimbert-Suriñach, Dr. J. Benet-Buchholz, Prof. A. Llobet

Institute of Chemical Research of Catalonia (ICIQ)
Barcelona Institute of Science and Technology
Av. Paisos Catalans 16, 43007 Tarragona (Spain)
E-mail: allobet@iciq.es

[b] Dr. M. Nippe, Prof. J. R. Long

Department of Chemistry, University of California
Berkeley, CA 94720 (USA)
E-mail: jrlong@berkeley.edu

[c] Dr. M. Nippe, Prof. J. R. Long

Materials Sciences Division, Lawrence Berkeley National Laboratory
Berkeley, CA 94720 (USA)

[d] Dr. X. Sala, Prof. A. Llobet

Departament de Química, Universitat Autònoma de Barcelona
Cerdanyola del Vallès, 08193 Barcelona (Spain)
E-mail: xavier.sala@uab.es

[e] Dr. M. Nippe

Department of Chemistry, Texas A&M University
College Station, TX 77840 (USA)

Supporting information for this article is available on the WWW under <http://dx.doi.org/10.1002/chem.201503567>.

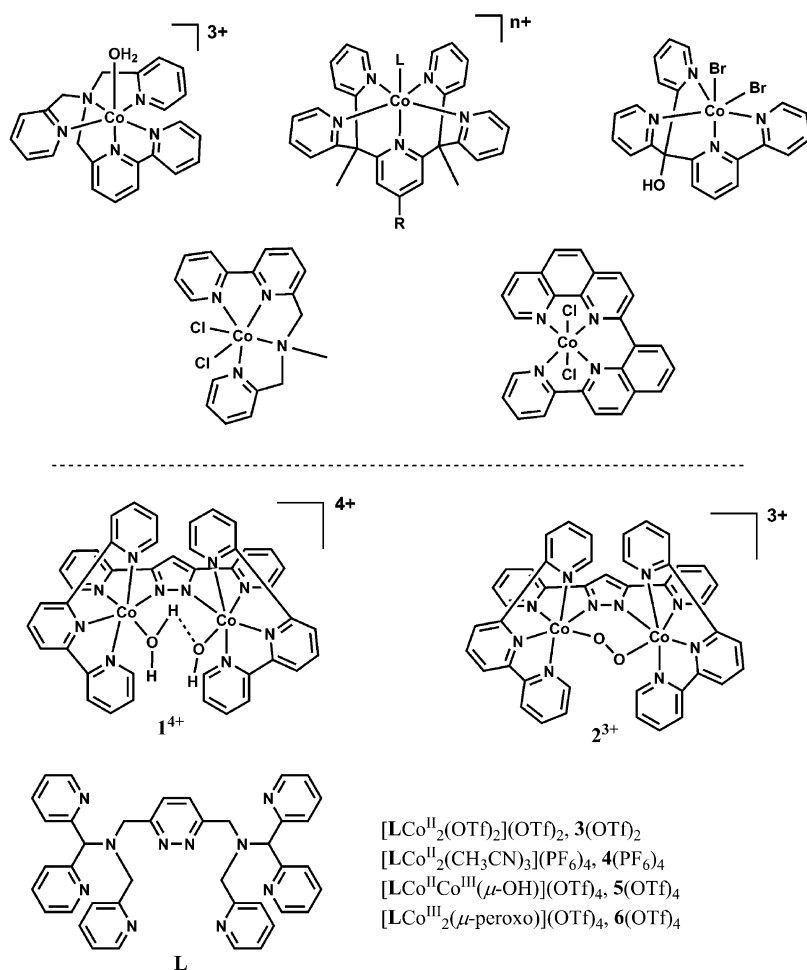
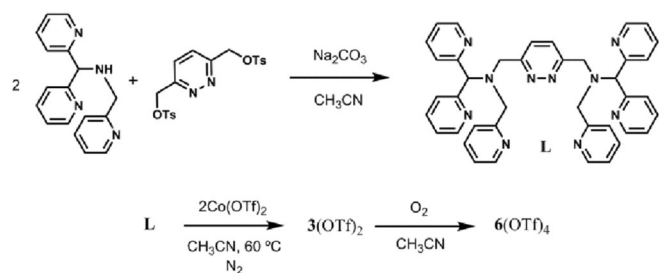


Figure 1. Top: Selected mononuclear cobalt HER catalysts of the polypyridinic ligand family reported in the literature.^[1h,k,l,t,5] Bottom: Dinuclear cobalt complexes for the HER (**1**⁴⁺)^[2] and ORR (**2**³⁺)^[3] reported in the literature and the complexes synthesized in this work (**3–6**).



Scheme 1. Synthesis of decadentate ligand **L**, complexes **3**(OTf)₂ and **6**(OTf)₄.

commodate small ligands such as chloro, acetonitrile, water, or bridging groups like hydroxo and peroxo ligands.

The synthesis of dicobalt complex **3**(OTf)₂ (OTf = ⁻OSO₂CF₃) was performed inside a N₂-filled glovebox by reacting ligand **L** with two equivalents of Co(OTf)₂ in acetonitrile at 60 °C. The mixture was filtered and the product precipitated by addition of diethyl ether. The pale-brown solid obtained was characterized by elemental analysis and ESI(+)-mass spectrometry. Both analyses agreed with a dinuclear complex of formula

[LCo^{II}₂(OTf)₂](OTf)₂ (**3**(OTf)₂), confirming the +2 oxidation state for the two metal centers.

Complex **3**²⁺ is highly air-sensitive in the solid state and in solution. Exposure to air results in a clear color change from pale brown to orange. Under strictly dry and anaerobic conditions, it was possible to obtain crystals of the Co^{II}₂ complex suitable for single-crystal X-ray diffraction studies by addition of ammonium hexafluorophosphate to an acetonitrile solution of **3**(OTf)₂. Figure 2A shows the molecular structure of **4**⁴⁺ in the crystalline solid **4**(PF₆)₄ with the formula [LCo^{II}₂(CH₃CN)₃](PF₆)₄, which is derived from substitution of two triflate ligands of the starting complex **3**²⁺ by two acetonitrile molecules and the partial dissociation of the pyridazine moiety. The N atom of a third acetonitrile molecule occupies the sixth coordination position of one of the metals, so that both cobalt atoms have a distorted octahedral geometry. The Co–N bond lengths are in the range 2.067(3)–2.224(3) Å, similar to those found in other polypyridine complexes of high-spin Co^{II} (Table S2 in the Supporting Information).^[1a,c,i] The asymmetric unit contains **4**⁴⁺, four PF₆⁻ anions, and three and a half co-crystallized acetonitrile molecules. The flexibility of the ligand provided by the backbone CH₂ groups, as well as the free rotation of the tertiary amine, may lead to the formation of a mix-

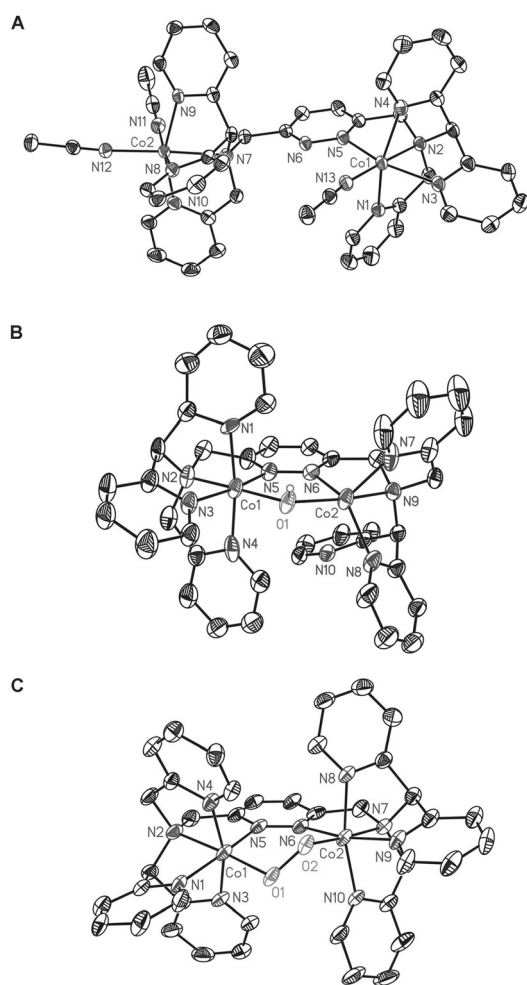


Figure 2. Thermal ellipsoid plots of the structures of: A) 4^{4+} (thermal ellipsoids at 50% probability level); B) 5^{4+} (thermal ellipsoids at 30% probability level); C) 6^{4+} (thermal ellipsoids at 30% probability level). Carbon-bonded H atoms are omitted for clarity.

ture of compounds in solution, in which the ligand and solvent compete for coordination sites at the metal centers.

Slow diffusion of hexanes into a benzonitrile (PhCN) solution of $3(\text{OTf})_2$ yielded single crystals of $[5^{4+}][\text{PF}_6]_4 \cdot \text{PhCN}$. The molecular structure of 5^{4+} features a μ_2 -OH bridge between the two Co centers (Figure 2B). The presence of four counter anions together with the two different Co–O bond lengths observed, that is, 1.889(18) Å and 1.963(17) Å for Co(1)–O(1) and Co(2)–O(1), respectively, are indicative of mixed-valent Co ions in 5^{4+} . Consistent with this hypothesis, the Co–N distances of the cobalt in oxidation state +3 are shorter than those of the cobalt in oxidation state +2 (Table S2 in the Supporting Information). Partial oxidation of the Co^{II} ions is likely due to trace amounts of oxygen and water present over the long crystallization time. Compound $5(\text{OTf})_4$ features one hexacoordinate Co^{III} center with the L ligand binding in a pentadentate manner and an O atom from a μ -OH group completing its first coordination sphere and bridging to a Co^{II} center. The latter is pentacoordinate, with one pendant pyridine of the L ligand, which functions here as a tetradentate ligand. Both $\text{Co}^{\text{III}}\text{--N}$ and $\text{Co}^{\text{III}}\text{--O}$ bond lengths are similar to those of related μ -OH

mixed-valence Co complexes,^[8] and these are summarized in Table S2.

The different geometries and coordination environments observed in the solid-state structures of 4^{4+} and 5^{4+} clearly emphasize the lability of interactions of L with divalent metal ions such as Co^{II} . The observed flexibility is key for the understanding of the electrochemical properties of 3^{2+} and its performance in redox catalysis (see below).

Complex $3(\text{OTf})_2$ can be oxidized under aerobic conditions to give a Co^{III} complex with the formula $[\text{LCo}^{\text{III}}_2(\mu\text{-peroxo})](\text{OTf})_4$ in quantitative yield ($6(\text{OTf})_4$, Scheme 1). Complex 6^{4+} is diamagnetic, as evident from its ^1H NMR spectroscopy (Figure S3 in the Supporting Information). Slow diffusion of diethyl ether into a solution of $6(\text{OTf})_4$ in ethanol resulted in crystals suitable for X-ray diffraction studies. The oxidized compound consists of a peroxo-bridged dinuclear $\text{Co}^{\text{III}}\text{Co}^{\text{III}}$ complex (Figure 2C). Both metal centers are hexacoordinated and have similar Co–N bond lengths that are within the range of expected values for octahedral Co^{III} complexes. The Co–O and O–O bond lengths were similar to those previously reported for complex 2 (Figure 1) and other peroxo-bridged dicobalt complexes.^[3,9,10] Crystallographic data and selected bond lengths and angles are listed in Tables S1 and S2 in the Supporting Information.

Redox chemistry of $3(\text{OTf})_2$ and $6(\text{OTf})_4$

The redox properties of complexes 3^{2+} and 6^{4+} were investigated by cyclic voltammetry (Figures 3 and 4). Cathodic scans reveal two quasi-reversible reductive waves at $E_c^1 = -1.00$ V and $E_c^2 = -1.14$ V for complex 3^{2+} (all potentials are given vs. the SCE reference electrode). These processes are attributed to two consecutive one-electron reductions of $\text{Co}^{\text{II}}\text{Co}^{\text{II}}$ to $\text{Co}^{\text{II}}\text{Co}^{\text{I}}$ and $\text{Co}^{\text{II}}\text{Co}^{\text{I}}$ to $\text{Co}^{\text{I}}\text{Co}^{\text{I}}$, respectively, and likely indicate weak electronic communication between the two cobalt centers through the pyridazine bridge. The reduction waves observed at more negative potentials (< -1.4 V) are tentatively assigned to processes involving the polypyridinic organic ligand L. In the oxidative scan of the voltammogram, a very broad wave at $E_a^3 = 0.68$ V is observed, and is tentatively assigned to a two-electron oxidation of the $\text{Co}^{\text{II}}\text{Co}^{\text{II}}$ species to furnish a $\text{Co}^{\text{III}}\text{Co}^{\text{III}}$ complex. The poor reversibility of the waves in both reduction and oxidation scan areas is a consequence of the flexible nature of the ligand, which induces variability of the coordination environment of the cobalt centers upon changing their oxidation state. On the other hand, $\text{Co}^{\text{III/II}}$ couples are frequently observed as broad features, which has been explained by the large reorganization energy associated with the change in spin-state in going from high-spin Co^{II} to low-spin Co^{III} and vice versa.^[11]

Figure 3B shows a cyclic voltammogram of a solution of complex 3^{2+} before and after addition of *p*-toluenesulfonic acid (*p*-TsOH). A catalytic wave appears at a potential slightly more positive than the first electron reduction at $E_c^1 = -1.00$ V, which increases upon increasing the concentration of the proton source. These results suggest that complex 3^{2+} may be an active catalyst for the HER and that the active species is a re-

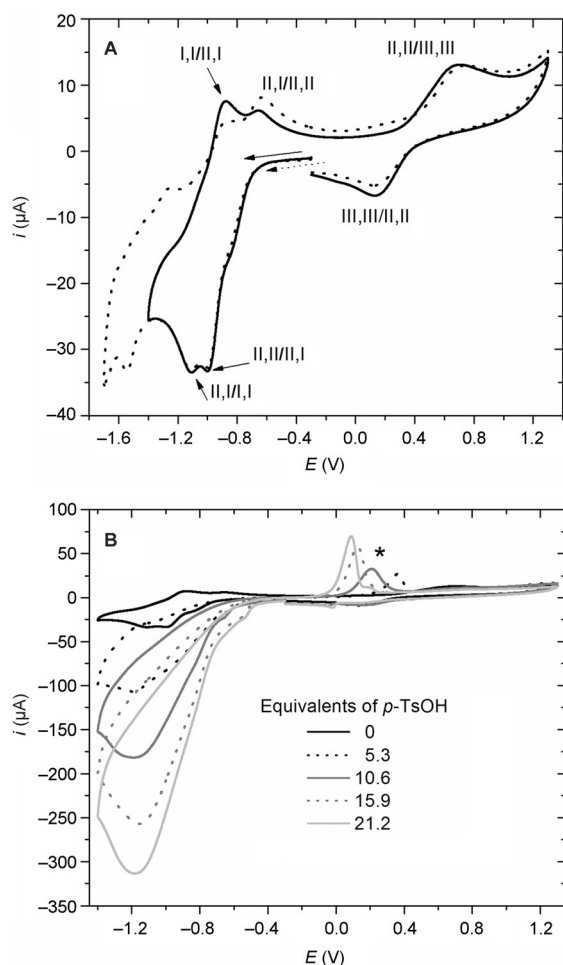


Figure 3. Cyclic voltammograms of a 1.4 mM solution of 3^{2+} in CH_3CN containing 0.1 M $[(n\text{Bu})_4\text{N}][\text{PF}_6]$ recorded inside a N_2 -filled glovebox; working electrode: glassy carbon; counter electrode: Pt; reference electrode: Ag/Ag^+ electrode in a solution of 0.01 M AgNO_3 in CH_3CN ; scan rate: 100 mVs^{-1} . A) In the absence of acid. B) In the presence of various amounts of p -TsOH. The asterisk indicates the formation of a surface-adsorbed species on the working electrode after the catalytic scan. See also Figure S4 in the Supporting Information.

duced Co^{I} intermediate, consistent with other reported Co-based molecular HER catalysts.^[12] We also note broad anodic stripping waves after catalytic reductive scans, which are indicative of oxidation of an adsorbed species. It is unclear if this species is molecular in nature or if a film is generated.^[13] It is therefore possible that electrocatalytic H_2 production does not solely involve the molecular homogeneous species under these experimental conditions. A one-hour bulk electrolysis experiment ($E_{\text{app}} = -0.75 \text{ V}$) employing a 5 mL acetonitrile solution containing 3^{2+} (1.4 mM) and p -TsOH acid (22 mM) afforded $11.1 \mu\text{mol}$ of hydrogen gas, accounting for 40% Faradaic efficiency (Figure S5 in the Supporting Information). Analogous experiments in the absence of 3^{2+} produced $1.3 \mu\text{mol}$ of hydrogen, proving the contribution of the catalyst in the hydrogen evolution reaction. The standard reduction potential of p -TsOH has previously been reported^[14] but more current studies highlight complications with standard potentials of organic acids in organic solvents.^[15] We therefore do not provide an es-

timate of the overpotential for HER of 3^{2+} under these conditions. Further evidence for the complexity of comparing hydrogen evolving catalysts in organic solvents with organic acids has been reported for a family of iron dimers and cobalt complexes containing pentadentate ligands.^[14, 16, 17]

The cyclic voltammogram of 6^{4+} in CH_3CN shows one reversible one-electron oxidative wave at $E_{1/2} = 1.67 \text{ V}$ (Figure 4), which is likely due to the formation of a $\text{Co}^{\text{III}}\text{Co}^{\text{IV}}$ species. There are also two reductive one-electron processes present, the first one at $E_c^1 = 0 \text{ V}$ is assigned to the $\text{Co}^{\text{III}}\text{Co}^{\text{III}}/\text{Co}^{\text{III}}\text{Co}^{\text{II}}$ couple. The lack of reversibility of the wave is probably due to cleavage of the O–O bond upon reduction.^[3] The second reduction wave at $E_c^2 = -0.38 \text{ V}$ is tentatively assigned to the reduction of a $\text{Co}^{\text{III}}\text{Co}^{\text{II}}$ to a $\text{Co}^{\text{II}}\text{Co}^{\text{II}}$ species and partial decomposition of the compound, giving byproducts that give rise to the features observed in the oxidative back scan (marked with an asterisk in Figure 4).

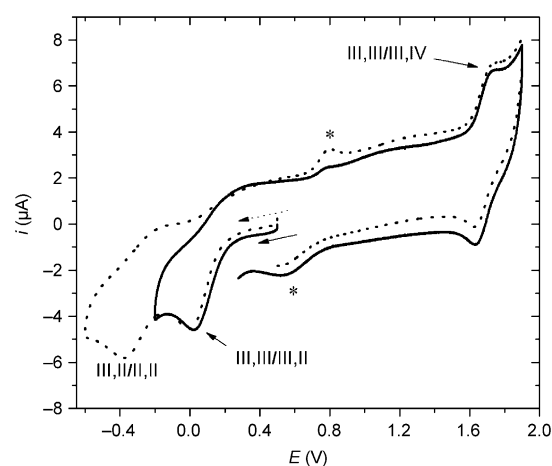


Figure 4. Cyclic voltammogram of a 0.5 mM solution of 6^{4+} in degassed CH_3CN containing 0.1 M $[(n\text{Bu})_4\text{N}][\text{PF}_6]$; working electrode: glassy carbon; counter electrode: Pt; reference electrode: SCE; scan rate: 100 mVs^{-1} . The asterisks correspond to species formed after the reductive scan.

All the potentials associated with the redox chemistry of 3^{2+} and 6^{4+} are summarized in Table 1, together with those of related catalysts 1^{4+} and 2^{3+} in Figure 1 for comparison. For complex 6^{4+} , the redox potentials are shifted anodically compared with those of 2^{3+} , an observation that is attributed to

Table 1. Summary of redox potentials for complexes 3^{2+} and 6^{4+} and reported complexes 1^{4+} and 2^{3+} (Figure 1).^[a]

Complex	$E_{c(\text{II,II,I})}$	$E_{c(\text{III,III,II})}$	$E_{c(\text{III,III,III})}$	$E_{c(\text{III,III,III,IV})}$	$E_{c(\text{IV,III,III,II})}$
1^{4+} ^[2]	-1.16 (qr)	1.08 (qr)	-0.04 (r)	0.31 (r)	-
$3(\text{OTf})_2$	-1.14 (qr)	1.00 (qr)	0.68 ($2e^-$, i)	-	-
2^{3+} ^[3]	-	-	-0.75 (i)	-0.27 (r)	1.47 (r)
$6(\text{OTf})_4$	-	-	-0.38 (qr)	0.00 (qr)	1.67 (r)

[a] All potentials are given in V vs. the SCE reference electrode. For the irreversible (i) and quasi-reversible (qr) couples, the value of the cathodic peak (E_c) or anodic peak (E_a) are given. For the reversible couples (r), the $E_{1/2}$ is given.

the neutral nature of ligand L compared with the monoanionic 3,5-bis(2-pyridyl)pyrazolate ligand in 2^{3+} . On the other hand, the reduction potentials of complexes 1^{4+} and 3^{2+} are very similar.

Photochemical hydrogen evolution reaction (HER) catalysis with complex $3(\text{OTf})_2$

The ability of complex 3^{2+} to catalyze proton reduction was tested under photochemical conditions in aqueous solution. According to the cyclic voltammograms shown in Figure 3, the potential required to generate the Co^{I} active species in acetonitrile is $E_c = -1.0 \text{ V}$. A cyclic voltammogram of 3^{2+} in water (pH 4.1, ascorbate buffer) shows onset of reductive current at -0.9 V (Figure S6 in the Supporting Information). These potentials are suitable to couple catalyst 3^{2+} with a $[\text{Ru}(\text{bpy})_3]^{2+}$ photosensitizer (PS; bpy = 2,2'-bipyridine), which has redox potentials of $E(\text{PS}/\text{PS}^-) = -1.33 \text{ V}$ and $E(\text{PS}^+/\text{PS}^*) = -1.1 \text{ V}$.^[11] Sodium ascorbate was chosen as the sacrificial electron donor as it is well known to effectively quench the excited state of $[\text{Ru}(\text{bpy})_3]^{2+}$.^[14,15] The hydrogen evolution profile obtained for the photochemical HER experiments using a mixture of the three components, $3(\text{OTf})_2$, $[\text{Ru}(\text{bpy})_3][\text{ClO}_4]_2$, and ascorbic acid/sodium ascorbate (1:1), at different concentrations and ratios are given in Figure 5. All reactions were performed at pH 4.1,

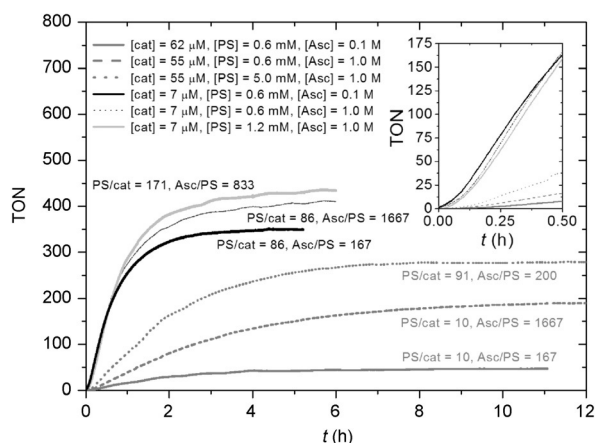


Figure 5. Hydrogen evolution catalysis profile using $3(\text{OTf})_2$, $[\text{Ru}(\text{bpy})_3][\text{ClO}_4]_2$ as photosensitizer, and ascorbic acid/sodium ascorbate (1:1) as sacrificial electron donor and buffered at pH 4.1. Reactions were performed in a 4 mL jacketed reactor at 25°C and using a 1.5 mL total volume of solution. Hydrogen gas evolution was monitored by using a Clark electrode. Turnover number (TON) = $\text{mol H}_2/\text{mol cat}$.

at 25°C , and under white-light illumination, calibrated to one sun intensity light.

At high concentrations of $3(\text{OTf})_2$ (55–62 μM), the catalytic activity of the system is highly dependent on the ascorbate/PS and PS/catalyst ratios, suggesting that the electron transfer from ascorbate to PS as well as that from PS to catalyst are limiting the performance of the reaction. These results support a reductive quenching mechanism in which the reduced photosensitizer intermediate (PS^-) is responsible for catalyst activation (Figure 6). Thus, the higher the ascorbate concentration

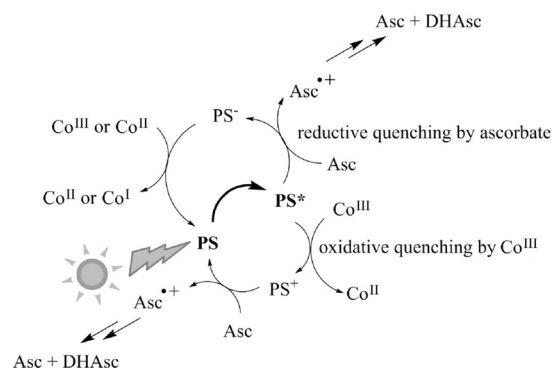


Figure 6. Plausible mechanisms for the photocatalytic activation of $3(\text{OTf})_2$ by $[\text{Ru}(\text{bpy})_3][\text{ClO}_4]_2$ photosensitizer (PS) and ascorbic acid/sodium ascorbate (Asc) sacrificial electron donor, based on experimental results and other reports in the literature.^[11h,k-m,o,s-u] Note that the oxidative quenching is only favored for the reduction of the Co^{III} intermediate species generated under turnover conditions, but not by the starting $\text{Co}^{\text{II}}\text{Co}^{\text{II}}$ complex because the reduction potential of the excited photosensitizer (PS^*) is too low to perform the first reduction from $\text{Co}^{\text{II}}\text{Co}^{\text{II}}$ to $\text{Co}^{\text{I}}\text{Co}^{\text{I}}$ ($E(\text{PS}^+/\text{PS}^*) = -1.08 \text{ V}$ vs. $E_c^1 = -0.9 \text{ V}$).

and ascorbate/PS or PS/catalyst ratios, the faster the reaction evolves.

On the other hand, a great enhancement of the catalytic rate and the turnover number of the reaction is observed when the catalyst concentration is lowered to $7 \mu\text{M}$. It has been reported that related mononuclear cobalt catalysts of the polypyridinic ligand family also perform better when the concentration of catalyst is $< 10 \mu\text{M}$.^[11h,11,5] Sometimes this behavior has been related to the deactivation of the catalyst as a result of formation of polynuclear cobalt species and higher nuclearity aggregates, which is favored at high concentrations of catalyst. Indeed, we observed the formation of cobalt nanoparticles in centrifuged crude catalytic mixtures with $[\text{cat}] = 55 \mu\text{M}$. The recycled nanoparticles were tested as potential catalysts in fresh mixtures containing PS and ascorbate, but only traces of hydrogen gas were detected (Figure S7 and Table S3 in the Supporting Information). Here, it is important to mention the contributions of other decomposition pathways that can lead to photocatalysis deactivation. These include photosensitizer decomposition and the accumulation of dehydroascorbate (DHAsc in Figure 6), the two-electron oxidation product of ascorbate, which has been shown to have a dramatic effect on the long-term stability of such systems.^[1e]

As pointed out before, at high concentrations of catalyst the system is limited by the electron transfers from ascorbate to PS and from PS to catalyst. This is not the case for the reaction containing $7 \mu\text{M}$ of catalyst, in which the initial catalytic rate does not improve when PS and ascorbate concentrations are increased (Figure 5, inset). Instead, under low catalyst concentration, the mechanism of the cobalt dark catalysis determines the speed of the overall reaction. Given the proven flexibility and lability of the ligand in complex $3(\text{OTf})_2$, it is likely that the two cobalt centers will interact with protons independently from each other, following an analogous mechanism to that of mononuclear cobalt polypyridine complexes such as those in Figure 1.^[11h,1,5] In most of the reported cases, heterolytic cleav-

age of Co^{III}–H bonds through protonation is the dominant mechanism for the evolution of H₂. The related dinuclear complex **1**⁴⁺ in Figure 1 was also found to undergo cleavage of the Co^{III}–H bond by protonation in acetonitrile solutions.^[2,12]

Chemical oxygen reduction reaction (ORR) catalysis with complex **6**(OTf)₄

The reduction of O₂ by octamethylferrocene (Me₈Fc) occurred with a catalytic amount of **6**⁴⁺ in the presence of TFA (trifluoroacetic acid) in acetonitrile at 298 K (Figure 7 and Fig-

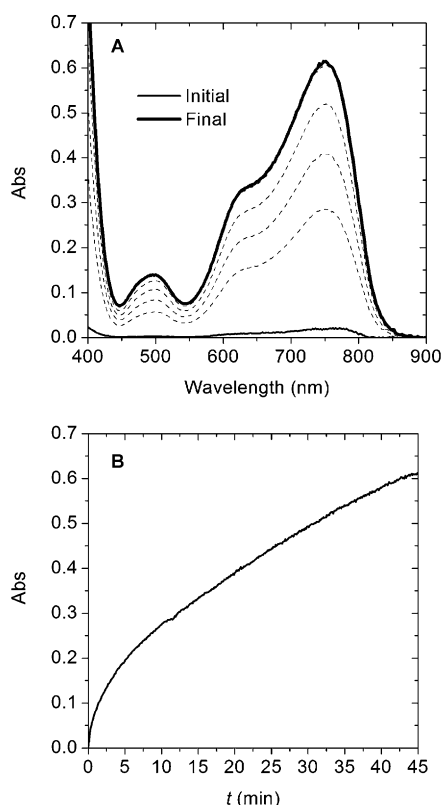


Figure 7. A) Absorption spectral changes in the two-electron reduction of O₂ by Me₈Fc (1.5×10^{-3} M) catalyzed by **6**⁴⁺ (2.5×10^{-5} M) in the presence of CF₃COOH (5.0×10^{-2} M) in O₂-saturated CH₃CN at 298 K. B) Time profile of the absorbance at λ = 750 nm resulting from the formation of Me₈Fc⁺.

ure S8 in the Supporting Information), with complete conversion of Me₈Fc to Me₈Fc⁺ ($\lambda_{\text{max}} = 750$ nm, $\epsilon = 410$ M⁻¹ cm⁻¹). Iodometric titrations confirmed that H₂O₂ was formed after the reaction was complete (Figure S9 in the Supporting Information). Thus, **6**⁴⁺ catalyzes the two-electron reduction of O₂ by Me₈Fc in the presence of TFA in acetonitrile following the stoichiometry shown in Equation (1). It is interesting to point out the difference in reactivity between **6**⁴⁺ and complex **2**³⁺ in Figure 1, which is able to catalyze the four-electron reduction of O₂ all the way to water by means of proton-coupled electron-transfer processes [Eq. (2)].^[3]



We have already mentioned the difference between the electrochemistry of both compounds (Table 1), mainly related to the monoanionic nature of the 3,5-bis(2-pyridyl)pyrazolate ligand in **2**³⁺ compared with the neutral nature of L in **6**(OTf)₄. Another important difference in their redox chemistry is related to the reversibility of the first reduction wave corresponding to a metal-centered reaction from Co^{III}Co^{III} to Co^{III}Co^{II}. Although this wave is reversible in **2**³⁺, it is quasi-reversible for **6**(OTf)₄, indicative of a chemical process or change in geometry after the reduction for **6**(OTf)₄. We were unable to perform kinetics studies of the reduction process in Figure 7 owing to the mixture of intermediates involved in the reaction, derived from the lability of the pyridine and pyridazine moieties in ligand L. The different behavior of **2**³⁺ with regards to **6**⁴⁺ emphasizes how subtle ligand variations can influence metal ion geometry and electron donation, which results in radically different reactivity.

Conclusion

We have synthesized a new decadentate dinucleating ligand, L, that can coordinate two metal ions in close proximity, as well as mediate electronic coupling. Four new dinuclear cobalt complexes featuring this ligand have been prepared and shown to exhibit different coordination modes and contain oxo and peroxo bridges, as ascertained by single-crystal X-ray diffraction analysis.

We have also shown that electrocatalytic hydrogen evolution in organic media is enhanced in the presence of complex **3**²⁺. In addition, we proved the capacity of this complex to undergo photochemically induced proton reduction catalysis in the presence of a dye, [Ru(bpy)₃]²⁺, and a sacrificial electron donor, ascorbate. The results obtained here are compared with those previously reported for the related polypyridine complexes shown in Figure 1. We have also shown that one of the deactivation processes in the photochemically induced reaction involves the formation of Co⁰ nanoparticles, as demonstrated by TEM images of the centrifuged final crude mixture.

Furthermore, complex **6**⁴⁺ was shown to act as a catalyst for the two-electron reduction of oxygen to give hydrogen peroxide, in sharp contrast to the related complex **2**³⁺, which reduces O₂ all the way to H₂O under comparable conditions. These results highlight how small changes to the ligand's electronic and geometrical properties can strongly influence the metal reactivity.

Experimental Section

Materials

All reagents used in the present work were obtained from Aldrich Chemical Co. or Alfa Aesar and were used without further purification. Synthesis-grade organic solvents were obtained from SDS and were routinely degassed with argon. Methanol (MeOH) was distilled over Mg/I₂, ethanol was dried with 3.5 Å molecular sieves,

and acetonitrile, dichloromethane, hexane, and diethyl ether were used from a solvent purification system. High-purity deionized water was obtained by passing distilled water through a nanopure Milli-Q water purification system. The ligand precursors 3,6-bis(tosyloxymethyl)pyridazine⁶ and *N*-[di(2-pyridinyl)methyl]-*N*-(2-pyridinylmethyl)amine⁷ were prepared by following procedures described in the literature. All synthetic manipulations were routinely performed under an argon atmosphere by using Schlenk and vacuum-line techniques.

***N,N'*-(Pyridazine-3,6-diylbis(methylene))bis(1,1-di(pyridin-2-yl)-*N*-(pyridin-2-ylmethyl)methanamine) (L)**

N-[Di(2-pyridinyl)methyl]-*N*-(2-pyridinylmethyl)amine (6.19 g, 22.4 mmol) and Na₂CO₃ (25 g, 236 mmol) were dissolved in dry acetonitrile (70 mL) and warmed at 50 °C under Ar. A solution of 3,6-bis(tosyloxymethyl)pyridazine (5.00 g, 11.1 mmol) in dry acetonitrile (150 mL) was added. The resulting solution was heated at reflux for 6 h under Ar. The crude was purified by chromatography (silica; washed with dichloromethane and eluted with dichloromethane/methanol 20:1) to give 3.20 g (4.87 mmol, yield: 44%) of pure product. ¹H NMR (400 MHz, CDCl₃): δ = 8.63–8.51 (m, 4H; H6, H11, H26, H31), 8.45 (d, *J* = 4.7 Hz, 2H; H16, H36), 7.70 (s, 2H; H1, H21), 7.68–7.61 (m, 8H; H8, H9, H13, H14, H28, H29, H33, H34), 7.58–7.47 (m, 4H; H18, H19, H38, H39), 7.17–7.09 (m, 4H; H7, H12, H27, H32), 7.06–6.97 (m, 2H; H17, H37), 5.26 (s, 2H; H4, H24), 4.10 (s, 4H; H3, H23), 3.92 ppm (s, 4H; H5, H25); ¹³C NMR (100 MHz, CDCl₃): δ = 160.64 (C2, C22), 159.84 (C10, C15, C30, C35), 159.47 (C20, C40), 149.44 (C6, C11, C26, C31), 149.18 (C16, C36), 136.50 (C9, C14, C29, C34), 136.46 (C19, C39), 127.11 (C1, C21), 124.29 (C8, C13, C28, C33), 123.46 (C18, C38), 122.36 (C7, C12, C27, C32), 122.02 (C17, C37), 72.59 (C4, C24), 57.79 (C5, C25), 55.45 ppm (C3, C23); (+)-ESI-MS: *m/z* = 657 for [L + H]⁺ and *m/z* = 679 for [L + Na]⁺.

{[Co^{II}(L)(OTf)₂]}(OTf)₂·5H₂O (3(OTf)₂·5H₂O)

The whole synthesis was carried out inside a glovebox with a N₂ atmosphere. [Co(OTf)₂]·0.5CH₃CN (80 mg, 0.21 mmol) and L (70 mg, 0.11 mmol) were dissolved in acetonitrile (2 mL) and warmed at 60 °C. The solution was stirred for 3 h at this temperature and then filtered through cotton wool to remove unreacted starting materials. The product was precipitated by addition of diethyl ether. The initial precipitate, in the form of oil, was scratched until a light-brown solid was obtained (125 mg, 0.091 mmol, 84%). HR-(+)-ESI-MS: *m/z* calcd for [Co^{II}(L)(OTf)₂]²⁺: 536.0414; found: 536.0470; elemental analysis calcd (%) for C₄₄H₃₆Co₂F₁₂N₁₀O₁₂S₄·5H₂O: C 36.17, H 3.17, N 9.59, S 8.78; found: C 36.38, H 3.09, N 9.26, S 8.48.

Crystals of 4(PF₆)₄ were grown under strictly dry and anaerobic conditions by slow evaporation of an acetonitrile solution of 3²⁺ at –30 °C. The addition of a drop of a saturated NH₄PF₆ methanol solution proved necessary for the growth of crystals of 4(PF₆)₄ suitable for X-ray diffraction.

Crystals of 5(PF₆)₄ were grown by slow diffusion of *n*-hexane into a solution of 3²⁺ in benzonitrile. The asymmetric unit contains one molecule of the complex, four triflate anions, and some highly disordered solvent molecules (probably benzonitrile).

{[Co^{III}(O-O)(L)]}(OTf)₄ (6(OTf)₄)

3(OTf)₂·5H₂O (30 mg) was left under aerobic conditions for one night. The red solid obtained was recrystallized from ethanol/diethyl ether, leading to the formation of dark-orange crystals (24 mg,

quantitative yield). ¹H NMR (400 MHz, CD₃CN): δ = 10.48 (d, *J* = 7.0 Hz, 1H; H40), 9.23 (d, *J* = 5.6 Hz, 1H; H34), 8.14–7.06 (m, 2H; H32, H31), 8.02 (td, *J* = 7.7, 1.44 Hz, 1H; H38), 7.95–7.88 (m, 2H; H26, H27), 7.76 (s, 1H; H2), 7.68–7.58 (m, 2H; H39, H33), 7.39 (d, *J* = 8.8 Hz, 1H; H37), 7.05 (d, *J* = 6.5 Hz, 1H; H29), 6.86 (s, 1H; H24), 6.79 (td, *J* = 6.54, 1.68 Hz, 1H; H28), 5.55 (d, *J* = 19.8 Hz, 1H; H35A), 5.50 (d, *J* = 20.39 Hz, 1H; H5A), 5.31 (d, *J* = 19.8 Hz, 1H; H35B), 5.21 ppm (d, *J* = 20.39 Hz, 1H; H5B); ¹³C NMR (100 MHz, CD₃CN): δ = 177.02 (C1), 167.62 (C36), 158.17 (C25, C30), 154.53 (C29), 154.12 (C34), 154.07 (C40), 143.57 (C32), 143.25 (C26), 142.35 (C38), 138.34 (C33), 132.51 (C2), 127.34 (C28), 127.21 (C39), 126.94 (C31), 126.41 (C27), 123.86 (C37), 78.11 (C24), 67.27 (C35), 66.05 ppm (C5).

Equipment and measurements

All electrochemical experiments were performed with a PAR 263A EG&G potentiostat or IJ-Cambria HI-660 potentiostat, using a three-electrode configuration electrochemical cell. Glassy carbon (3 mm diameter) from BAS was used as the working electrode, a platinum wire as the auxiliary electrode, and SSCE (NaCl sat.) or Ag/AgNO₃ (0.01 M in CH₃CN) as reference electrode. Cyclic voltammograms were recorded at a 100 mV s⁻¹ scan rate. The complexes were dissolved in previously degassed CH₃CN containing the necessary amount of [(*n*Bu₄N)](PF₆), used as the supporting electrolyte, to yield a 0.1 M ionic strength solution. All *E*_{1/2} values reported in this work were estimated from cyclic voltammetry (CV) as the average of the oxidative and reductive peak potentials (*E*₃ + *E*₂)/2 or from differential pulse voltammetry (DPV; pulse amplitudes of 0.05 V, pulse widths of 0.05 s, sampling width of 0.02 s, and a pulse period of 0.1 s). A 400 MHz Bruker Avance II spectrometer and a Bruker Avance 500 MHz were used to carry out NMR spectroscopy at room temperature. Elemental analyses were performed by using a Carlo Erba CHMS EA–1108 instrument provided by the Chemical Analysis Service of the Universitat Autònoma de Barcelona (CAS-UAB).

Single-crystal X-ray structure determination

The crystals were measured under inert conditions by immersion in perfluoropolyether as the protecting oil for manipulation. Data collection: Crystal structure determination for 4(PF₆)₄ and 6(PF₆)₄ were carried out by using a Bruker-Nonius diffractometer equipped with an APPEX 2 4K CCD area detector, a FR591 rotating anode with Mo_{Kα} radiation, Montel mirrors as monochromator, and an Oxford Cryosystems low-temperature device Cryostream 700 plus (*T* = –173 °C). Crystal structure determination for 5(OTf)₄ was carried out by using a Apex DUO diffractometer equipped with a Kappa 4-axis goniometer, an APEX II 4K CCD area detector, a Microfocus Source E025 luS using Mo_{Kα} radiation, Quazar MX multi-layer Optics as monochromator, and an Oxford Cryosystems low-temperature device Cryostream 700 plus (*T* = –173 °C). Full-sphere data collection was used with ω and φ scans. Programs used: Data collection APEX-2,^[18] data reduction Bruker Saint^[19] V/60A and absorption correction SADABS.^[20] Structure solution and refinement: Crystal structure solution was achieved by using direct methods as implemented in SHELXTL^[21] and visualized by using the program XP. Missing atoms were subsequently located from difference Fourier synthesis and added to the atom list. Least-squares refinement on *F*² using all measured intensities was carried out by using the program SHELXTL. All non-hydrogen atoms were refined, including anisotropic displacement parameters.

Electrochemical hydrogen evolution experiments with 3(OTf)₂ in acetonitrile

A two compartment cell separated with a frit was used to perform electrochemical proton reduction experiments (5 mL of solution per compartment). In the reduction side, the working electrode (glassy carbon rod) and reference electrode (Ag/AgCl) were immersed in a degassed acetonitrile solution containing [(nBu)₄N][PF₆] (0.1 M), 3(OTf)₂ (1.4 mM), and *p*-TsOH (22 mM). In the oxidation side, a platinum wire counter electrode was immersed in a degassed acetonitrile solution containing [(nBu)₄N][PF₆] (0.1 M). A bulk electrolysis at -0.75 V vs. SCE (-0.7 V vs. Ag/AgCl) was performed over a 1 h period. At the end of the electrolysis, the headspace of the reduction compartment was analyzed by gas chromatography with thermal conductivity detectors, and hydrogen gas (271 μL) was detected. Analogous reactions in the absence of catalyst 3(OTf)₂ produced 50 μL of hydrogen gas.

Photochemical hydrogen evolution experiments were performed with 3(OTf)₂ in aqueous solution (example given for [cat]=7 μM, [PS]=0.6 mM, and [Asc]=0.1 M). Inside a N₂-filled glovebox, 7 μL of a 1.4 mM solution of 3(OTf)₂ (0.01 μmol) in acetonitrile was transferred into a jacketed 4 mL flask, which was then sealed with a septum. Outside the glovebox, a mixture of ascorbic acid (20 mg, 1.1 × 10⁻⁴ mol), sodium ascorbate (21 mg, 1.1 × 10⁻⁴ mol), and [Ru(bpy)₃][ClO₄]₂ (0.94 mg, 1.22 mmol) in water (2 mL) was degassed for 30 min by bubbling nitrogen. After this time, 1.5 mL of the degassed solution was transferred into the jacketed flask containing the catalyst. A Clark hydrogen sensor was inserted in the cell and the mixture irradiated by using a 150 W Xe Arc Lamp with a cut-off filter (λ > 400 nm, 25 mm). The light intensity was calibrated to "1 sun" prior to the experiment and the temperature was kept constant at 25 °C. At the end of the experiment, the cell was degassed with nitrogen and calibrated by adding known amounts of hydrogen.

Chemical oxygen reduction with 6(OTf)₄

An oxygen-saturated solution of CH₃CN containing octamethylferrocene (Me₈Fc, 1.5 × 10⁻³ M) and trifluoroacetic acid (TFA, 5 × 10⁻² M) was prepared and the UV/Vis spectra measured as background. Complex 6⁴⁺ (2.5 × 10⁻⁵ M) was then added and the UV/Vis spectra recorded by following the formation of Me₈Fc⁺ at λ = 750 nm. An analogous experiment in the absence of the catalyst was performed as a blank test. The amount of hydrogen peroxide formed was determined by titration with iodide ion: a diluted CH₃CN solution (2.0 mL) of the product mixture (50 μL) was treated with excess amount of NaI and the amount of I³⁻ formed was determined by the absorption spectrum (λ = 361 nm, ε = 2.8 × 10⁴ M⁻¹).

Acknowledgements

We thank MINECO (CTQ2011-2640, CTQ-2013-49075, SEV-2013-0319, CTQ-2014-52974-REDC), Feder funds and the EU COST actions CM1202 and CM1205. C.G.S. is grateful to AGAUR for a "Beatriu de Pinós" postdoctoral grant" and X.S. thanks AGAUR, Generalitat de Catalunya for a BE mobility grant.

Keywords: decadentate ligands · dicobalt complexes · oxygen reduction · peroxo bridges · proton reduction

[1] a) J. P. Bigi, T. E. Hanna, W. H. Harman, A. Chang, C. J. Chang, *Chem. Commun.* **2010**, 46, 958–960; b) C.-F. Leung, Y.-Z. Chen, H.-Q. Yu, S.-M.

- Yiu, C.-C. Ko, T.-C. Lau, *Int. J. Hydrogen Energy* **2011**, 36, 11640–11645; c) Y. Sun, J. P. Bigi, N. A. Piro, M. L. Tang, J. R. Long, C. J. Chang, *J. Am. Chem. Soc.* **2011**, 133, 9212–9215; d) W. T. Eckenhoff, R. Eisenberg, *Dalton Trans.* **2012**, 41, 13004–13021; e) M. Guttentag, A. Rodenberg, R. Kopelent, B. Probst, C. Buchwalder, M. Brandstätter, P. Hamm, R. Alberto, *Eur. J. Inorg. Chem.* **2012**, 59–64; f) C.-F. Leung, S.-M. Ng, C.-C. Ko, W.-L. Man, J. Wu, L. Chen, T.-C. Lau, *Energy Environ. Sci.* **2012**, 5, 7903–7907; g) C. C. L. McCrory, C. Uyeda, J. C. Peters, *J. Am. Chem. Soc.* **2012**, 134, 3164–3170; h) W. M. Singh, T. Baine, S. Kudo, S. Tian, X. A. N. Ma, H. Zhou, N. J. DeYonker, T. C. Pham, J. C. Bollinger, D. L. Baker, B. Yan, C. E. Webster, X. Zhao, *Angew. Chem. Int. Ed.* **2012**, 51, 5941–5944; *Angew. Chem.* **2012**, 124, 6043–6046; i) C. Bachmann, M. Guttentag, B. Spingler, R. Alberto, *Inorg. Chem.* **2013**, 52, 6055–6061; j) A. E. King, Y. Surendranath, N. A. Piro, J. P. Bigi, J. R. Long, C. J. Chang, *Chem. Sci.* **2013**, 4, 1578–1587; k) B. Shan, T. Baine, X. A. N. Ma, X. Zhao, R. H. Schmehl, *Inorg. Chem.* **2013**, 52, 4853–4859; l) W. M. Singh, M. Mirmohades, R. T. Jane, T. A. White, L. Hammarstrom, A. Thapper, R. Lomoth, S. Ott, *Chem. Commun.* **2013**, 49, 8638–8640; m) Y. Sun, J. Sun, J. R. Long, P. Yang, C. J. Chang, *Chem. Sci.* **2013**, 4, 118–124; n) V. S. Thoi, Y. Sun, J. R. Long, C. J. Chang, *Chem. Soc. Rev.* **2013**, 42, 2388–2400; o) S. Varma, C. E. Castillo, T. Stoll, J. Fortage, A. G. Blackman, F. Molton, A. Deronzier, M.-N. Collomb, *Phys. Chem. Chem. Phys.* **2013**, 15, 17544–17552; p) C. Bachmann, B. Probst, M. Guttentag, R. Alberto, *Chem. Commun.* **2014**, 50, 6737–6739; q) A. Call, Z. Codolà, F. Acuña-Parés, J. Lloret-Fillol, *Chem. Eur. J.* **2014**, 20, 6171–6183; r) E. Deponti, A. Luisa, M. Natali, E. Iengo, F. Scandola, *Dalton Trans.* **2014**, 43, 16345–16353; s) C. Gimbert-Suriñach, J. Albero, T. Stoll, J. Fortage, M.-N. Collomb, A. Deronzier, E. Palomares, A. Llobet, *J. Am. Chem. Soc.* **2014**, 136, 7655–7661; t) R. S. Khnayzer, V. S. Thoi, M. Nippe, A. E. King, J. W. Jurss, K. A. El Roz, J. R. Long, C. J. Chang, F. N. Castellano, *Energy Environ. Sci.* **2014**, 7, 1477–1488; u) M. Natali, A. Luisa, E. Iengo, F. Scandola, *Chem. Commun.* **2014**, 50, 1842–1844; v) J. Xie, Q. Zhou, C. Li, W. Wang, Y. Hou, B. Zhang, X. Wang, *Chem. Commun.* **2014**, 50, 6520–6522; w) A. Rodenberg, M. Oraziotti, B. Probst, C. Bachmann, R. Alberto, K. K. Baldrige, P. Hamm, *Inorg. Chem.* **2015**, 54, 646–657.
- [2] S. Mandal, S. Shikano, Y. Yamada, Y.-M. Lee, W. Nam, A. Llobet, S. Fukuzumi, *J. Am. Chem. Soc.* **2013**, 135, 15294–15297.
- [3] S. Fukuzumi, S. Mandal, K. Mase, K. Ohkubo, H. Park, J. Benet-Buchholz, W. Nam, A. Llobet, *J. Am. Chem. Soc.* **2012**, 134, 9906–9909.
- [4] a) P. W. Ball, A. B. Blake, *J. Chem. Soc. Dalton Trans.* **1974**, 852–859; b) D. V. Bautista, J. C. Dewan, L. K. Thompson, *Can. J. Chem.* **1982**, 60, 2583–2593; c) J. C. Dewan, L. K. Thompson, *Can. J. Chem.* **1982**, 60, 121–132; d) M. Ghedini, G. De Munno, G. Denti, A. M. M. Lanfredi, A. Tiripicchio, *Inorg. Chim. Acta* **1982**, 57, 87–93; e) G. Marongiu, E. C. Lingafelter, *Acta Crystallogr. Sect. B* **1982**, 38, 620–622; f) G. Bullock, F. W. Hartstock, L. K. Thompson, *Can. J. Chem.* **1983**, 61, 57–62; g) L. K. Thompson, *Can. J. Chem.* **1983**, 61, 579–583; h) S. Brooker, R. J. Kelly, B. Moubaraki, K. S. Murray, *Chem. Commun.* **1996**, 2579–2580; i) S. Brooker, P. G. Plioger, B. Moubaraki, K. S. Murray, *Angew. Chem. Int. Ed.* **1999**, 38, 408–410; *Angew. Chem.* **1999**, 111, 424–426; j) S. Brooker, T. C. Davidson, S. J. Hay, R. J. Kelly, D. K. Kennepohl, P. G. Plioger, B. Moubaraki, K. S. Murray, E. Bill, E. Bothe, *Coord. Chem. Rev.* **2001**, 216–217, 3–30; k) U. Beckmann, S. Brooker, *Coord. Chem. Rev.* **2003**, 245, 17–29.
- [5] a) M. Guttentag, A. Rodenberg, C. Bachmann, A. Senn, P. Hamm, R. Alberto, *Dalton Trans.* **2013**, 42, 334–337; b) L. Tong, R. Zong, R. P. Thummel, *J. Am. Chem. Soc.* **2014**, 136, 4881–4884.
- [6] A. Picot, F. P. Gabbai, *Tetrahedron Lett.* **2002**, 43, 11–13.
- [7] G. Roelfes, M. E. Branum, L. Wang, L. Que, B. L. Feringa, *J. Am. Chem. Soc.* **2000**, 122, 11517–11518.
- [8] a) J. Luo, N. P. Rath, L. M. Mirica, *Inorg. Chem.* **2011**, 50, 6152–6157; b) Z. A. Siddiqi, A. Siddique, M. Shahid, M. Khalid, P. K. Sharma, Anjuli, M. Ahmad, S. Kumar, Y. Lan, A. K. Powell, *Dalton Trans.* **2013**, 42, 9513–9522.
- [9] K. Yamanari, M. Mori, S. Dogi, A. Fuyuhiko, *Inorg. Chem.* **1994**, 33, 4807–4809.
- [10] T. Tanase, T. Onaka, M. Nakagoshi, I. Kinoshita, K. Shibata, M. Doe, J. Fujii, S. Yano, *Inorg. Chem.* **1999**, 38, 3150–3159.
- [11] M. Nippe, R. S. Khnayzer, J. A. Panetier, D. Z. Zee, B. S. Olaiya, M. Head-Gordon, C. J. Chang, F. N. Castellano, J. R. Long, *Chem. Sci.* **2013**, 4, 3934–3945.

- [12] V. Artero, M. Chavarot-Kerlidou, M. Fontecave, *Angew. Chem. Int. Ed.* **2011**, *50*, 7238–7266; *Angew. Chem.* **2011**, *123*, 7376–7405.
- [13] B. D. McCarthy, C. L. Donley, J. L. Dempsey, *Chem. Sci.* **2015**, *6*, 2827–2834.
- [14] G. A. N. Felton, R. S. Glass, D. L. Lichtenberger, D. H. Evans, *Inorg. Chem.* **2006**, *45*, 9181–9184.
- [15] B. D. McCarthy, D. J. Martin, E. S. Rountree, A. C. Ullman, J. L. Dempsey, *Inorg. Chem.* **2014**, *53*, 8350–8361.
- [16] G. A. N. Felton, C. A. Mebi, B. J. Petro, A. K. Vannucci, D. H. Evans, R. S. Glass, D. L. Lichtenberger, *J. Organomet. Chem.* **2009**, *694*, 2681–2699.
- [17] J. W. Jurss, R. S. Khnayzer, J. A. Panetier, K. A. El Roz, E. M. Nichols, M. Head-Gordon, J. R. Long, F. N. Castellano, C. J. Chang, *Chem. Sci.* **2015**, *6*, 4954–4972.
- [18] Data collection with APEX II, version v2013.4-1, Bruker AXS Inc., Madison, Wisconsin, USA, **2007**.
- [19] Data reduction with Bruker SAINT, version V8.30c, Bruker AXS Inc., Madison, Wisconsin, USA, **2007**.
- [20] a) SADABS: V2012/1, Bruker AXS Inc., Madison, Wisconsin, USA, **2001**; b) R. H. Blessing, *Acta Crystallogr.* **1995**, *A51*, 33–38.
- [21] a) G. M. Sheldrick, *Acta Crystallogr. Sect. A* **2008**, *64*, 112–122; b) SHELXTL version V116.114.

Received: September 6, 2015

Published online on November 26, 2015